THE ASTROPHYSICAL JOURNAL, 423:674–680, 1994 March 10

INFRARED SPECTROSCOPY AND IMAGING POLARIMETRY OF THE DISK AROUND THE T TAURI STAR RNO 91

DAVID A. WEINTRAUB,[1,2,3] STEPHEN C. TEGLER,[3,4] JOEL H. KASTNER,[2,5,6] AND TERRENCE RETTIG[3,4]
Received 1993 May 7; accepted 1993 September 20

ABSTRACT

We present 3–5 μm spectra and a 2.2 μm polarimetric image of the T Tauri star RNO 91. We report the detection of three absorption bands centered at 3250 cm^{-1} (3.08 μm), 2139 cm^{-1} (4.68 μm), and 2165 cm^{-1} (4.62 μm) in spectra of RNO 91. These features are due to frozen H_2O, CO, and possibly XCN along the line of sight toward RNO 91. Our 2187–2107 cm^{-1} spectrum of RNO 90, the only other T Tauri star in the dark cloud L43, does not show the CO or XCN absorption bands. By comparing our observed polarimetric image with modeled images of scattered light from bipolar nebulae or circumstellar disks as well as with known morphology of the RNO 91 bipolar outflow, we demonstrate that the reflection nebulosity seen in the near-infrared is most likely a circumstellar disklike structure with a radius of $\sim$1700 AU. The location of both RNO 90 and RNO 91 in front of or near the front of L43 suggests that the intracloud optical depths toward both stars are small and, therefore, that the frozen H_2O, CO, and XCN molecules are located on grains in circumstellar material around RNO 91 at distances from the central star of perhaps 10–1700 AU. This frozen material may represent precometary grains orbiting RNO 91.

Subject headings: circumstellar matter — infrared: stars — ISM: molecules — polarization — stars: individual (RNO 91) — stars: pre–main-sequence

1. INTRODUCTION

RNO 91, one of only two pre–main-sequence stars in the tiny, dark cloud L43, appears to be the exciting star for a molecular outflow that shows spatially separated redshifted and blueshifted lobes (Levreault 1988; Myers et al. 1988; Mathieu et al. 1988). The redshifted outflow lobe extends to the north; the blueshifted outflow lobe extends to the south. High-resolution optical images reveal that RNO 91 comprises a group of clumps (Schild, Weir, & Mathieu 1989), some of which are aligned close to the southern outflow, giving the appearance of a jet. Other clumps are aligned nearly perpendicular to the outflow axis. Schild et al. suggest these clumps may be attributed to a disk.

Strong Hα emission led Levreault (1988) to classify RNO 91 as an M0.5 T Tauri star. Spectra of the individual clumps show no evidence of any other emission lines (Schild et al. 1989). The spectra of the fainter clumps are identical to the spectra of the main peak of RNO 91. The lack of shock emission lines in the clumps and their spectral similarity to the main peak suggest that all of these minor intensity peaks are reflection nebulosities. Indeed, the peak identified as RNO 91 may also be a reflection nebula, and the actual star may be completely obscured at optical and near-infrared wavelengths. This interpretation may be supported by a 1.6 μm polarimetric map of the nebula (Heyer et al. 1990). Heyer et al. used this map to pinpoint the apparent position of the exciting star at $\sim$2″ southeast of the main peak of RNO 91.

In 1988, when Heyer et al. (1990) made the *H*-band map, the infrared array with which they made the images suffered from a readout resetting problem that rendered much of the published *J*, *H*, and *K*-band intensity maps and the *H*-band polarimetric map inaccurate. Weintraub et al. (1992) demonstrated that the contamination of polarimetric imaging data taken with this array was more severe than originally estimated by Heyer et al. Essentially all the information contained in pixels immediately south of a bright source (i.e., both the main and principal secondary peaks of RNO 91) are suspect, and some of the conclusions drawn from the data in the polarimetric map, such as the location of the exciting star, also must be reexamined.

Ice components are known to exist in comets (see Mumma, Weissman, & Stern 1993), dark clouds (e.g., Whittet et al. 1983; Tanaka et al. 1990; Chen & Graham 1993), shells around protostars (Willner et al. 1982; Tielens 1989) and, in a few cases, disks around T Tauri stars (Cohen 1975; Tegler et al. 1993a). Although the relative abundance of ice components in protostellar and cometary environments has been under study for several years, few such measurements have been made for material surrounding T Tauri stars. Ices in disks around T Tauri stars are intermediate in an evolutionary sense between interstellar ices around protostars and ices in comets; hence, such measurements may provide evidence for determining whether cometary ices form in disks or whether they survived in abundant enough quantities from interstellar reservoirs to permit comet formation without additional ice evolution. For pre–main-sequence stars, relative abundance measurements of frozen materials exist only for L1551 IRS 5 (Tegler et al. 1993a). If, as the radio morphology suggests, we view RNO 91 through an edge-on circumstellar disk, this T Tauri star is an excellent candidate for studying the relative abundance of ices in precometary disks.

High-resolution polarimetric imaging should clearly demonstrate whether the peaks that make up RNO 91 are dusty com-

[1] Department of Physics & Astronomy, Vanderbilt University, Nashville, TN 37235.
[2] Visiting Astronomer, National Optical Astronomy Observatories, Tucson, AZ, which is operated by Associated Universities for Research in Astronomy, Inc., for the National Science Foundation.
[3] Visiting Astronomer, Infrared Telescope Facility, Mauna Kea, HI, which is operated by the University of Hawaii under contract with the National Aeronautics and Space Administration.
[4] Department of Physics, University of Notre Dame, Notre Dame, IN 46556.
[5] MIT Haystack Observatory, NEROC, Route 40, Westford, MA 01886.
[6] Present address: MIT, Center for Space Research, 37-667a, Cambridge, MA 02139.

ponents of the bipolar outflow and of a disk viewed nearly edge-on to the disk plane, as suggested by Schild et al. (1989), and whether the optical and near-infrared peaks are dense portions of the surrounding medium seen in reflection. Therefore, we have undertaken and now present a K-band (2.2 μm) polarimetric imaging study of the RNO 91 nebula. In order to determine the relative abundance of H_2O, CO, and XCN ices in the possible circumstellar disk of RNO 91, we also carried out a low-resolution, 3–5 μm spectroscopic study of this nebula.

Our infrared spectra of RNO 91 reveal strong evidence for frozen water (H_2O) and frozen carbon monoxide (CO) in the dust associated with the disk. Our spectra also reveal possible evidence for a frozen compound in the disk containing a nitrile (—C≡N) or an iso-nitrile (C≡N—) group. In the following analysis our polarimetric maps show that most, and perhaps all, of the light from the secondary peaks in the RNO 91 nebula is scattered. The polarization centroid may be as much as 2″ directly south of the 2 μm peak; hence, light from the 2 μm peak may also be scattered. By comparing the polarimetric map to models generated by Whitney & Hartmann (1992, 1993), we show that the observed morphology can be explained as starlight scattered off a large circumstellar disk viewed at an angle inclined relative to our line of sight.

2. OBSERVATIONS

2.1. *Infrared Spectroscopy*

As part of our program to survey the identity and abundance of icy components such as H_2O, CO, and XCN in the environments around T Tauri stars, we obtained spectroscopic observations of RNO 90 and RNO 91 with the Cryogenic Array Spectrometer (CGAS) (Tokunaga, Smith, & Irwin 1987) and the NASA Infrared Telescope Facility (IRTF) on Mauna Kea, Hawaii, on 1992 April 20–22 and August 2–5 U.T. CGAS is a grating spectrometer with a linear array of 29 consecutive working InSb detectors. The observations were obtained with a 2.″7 circular aperture and a 20″ east–west chop. The spectrometer, used in first order with grating B for 2187–2145 cm^{-1} and 2157–2107 cm^{-1} spectra and in first order with grating A for 3540–2966 cm^{-1} and 3092–2644 cm^{-1} spectra, provided resolving powers of $\lambda/\Delta\lambda$ of $\simeq$1300 and $\simeq$150, respectively. Wavenumber calibration was obtained with krypton and argon lamps inside CGAS. Observations of both RNO 90 and RNO 91 were obtained at grating positions centered at 2132 cm^{-1} (4.690 μm) and 2169 cm^{-1} (4.610 μm). Because of time constraints, only RNO 91 was observed at two additional grating positions, centered at 3248 cm^{-1} (3.079 μm) and 2835 cm^{-1} (3.528 μm). In Table 1 we present the integration time per spectrum and the number of spectra at each grating tilt for RNO 90 and RNO 91, and the calibrator star BS 6147.

The spectra of RNO 90 and RNO 91 were sky-subtracted and divided by spectra of BS 6147. By restricting the airmass difference between the objects and BS 6147 to less than 0.10, we ensured that telluric absorption features were accurately removed. To achieved a relative flux calibration, the spectra of RNO 90 and RNO 91 were multiplied by a T = 5490 K blackbody appropriate for BS 6147. We connected the spectra centered at 2132 and 2169 cm^{-1} by matching the overlapping portions in the 2150 cm^{-1} region. The spectra centered at 3248 and 2835 cm^{-1} also were connected by matching the overlapping portions. The continuum was determined for each spectrum from a linear function. The linear function was determined from the average wavenumbers and fluxes of the first four and the last four data points.

TABLE 1

PARAMETERS FOR CGAS OBSERVATIONS

Object	Wavenumber Interval (cm^{-1})	Integration Time per Spectrum (s)	Number of Spectra
RNO 90	2187–2145	6	6
	2157–2107	7	7
BS 6147	2187–2145	6	2
	2157–2107	7	2
RNO 91	3540–2966	32	4
	3092–2644	16	4
	2187–2145	6	7
	2157–2107	16	6
BS 6147	3540–2966	32	1
	3092–2644	16	1
	2187–2145	6	3
	2157–2107	16	2

The calibrated spectra of RNO 91 show several absorption bands. The 3540–2644 cm^{-1} spectrum of RNO 91 (Fig. 1) reveals a deep (τ_{3250} = 1.29) and broad absorption band that peaks at 3250 cm^{-1} (3.08 μm). The calibrated 2187–2107 cm^{-1} spectrum of RNO 91 is plotted at full resolution in Figure 2*a* and at lower resolution in Figure 3. This spectrum shows a shallower absorption band (τ_{2139} = 0.33) at 2139 cm^{-1} (4.68 μm). This spectrum also appears to have a broad band centered near 2165 cm^{-1}, and extending from 2178 to 2156 cm^{-1}. This band is similar to that seen in the spectra of the FU Orionis star L1551 IRS 5 (plotted for comparison in Fig. 2*b*; from Tegler et al. 1993a) and of the protostars NGC 7538 IRS 9 and W33 A (see Fig. 5 of Tegler et al. 1993a). The statistical significance of each data point across this absorption profile is marginal, at the 1–1.5 σ level; however, the consistency of the pattern across 12 consecutive spectral points sug-

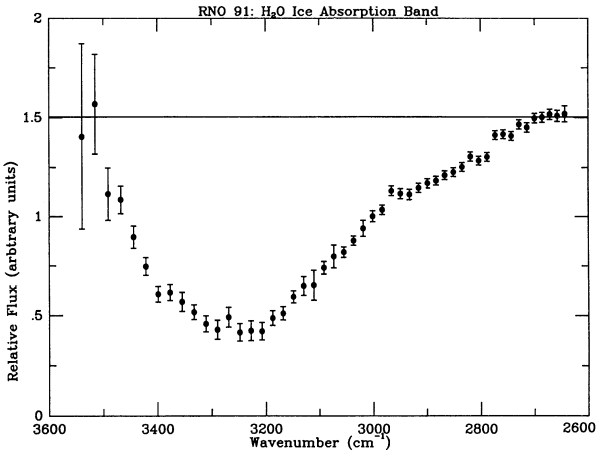

FIG. 1.—The 3540–2640 cm^{-1} spectrum of RNO 91. Flux is given in arbitrary units. The estimated continuum level is shown with the solid line. The strong, broad absorption band at 3250 cm^{-1} (3.08 μm) is attributed to the OH stretch of H_2O molecules frozen on the surfaces of grains in the disk around RNO 91.

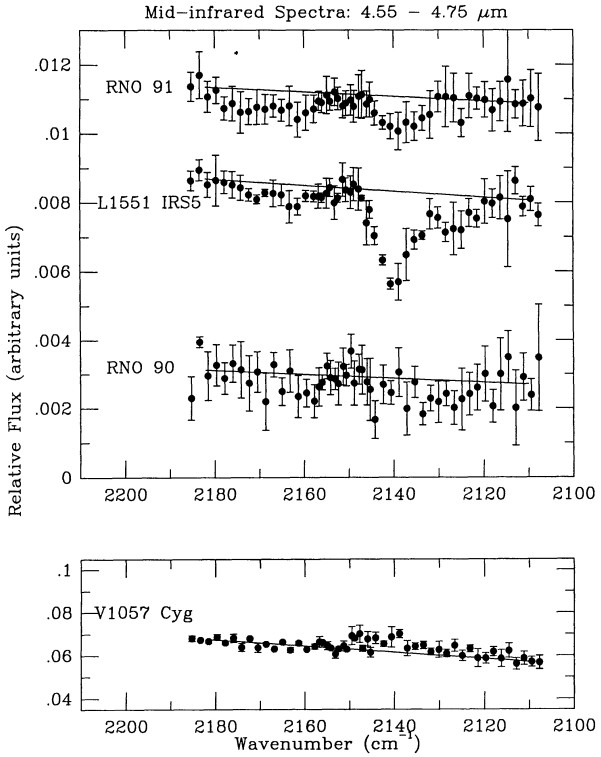

FIG. 2.—(*a*) Calibrated 2187–2107 cm^{-1} spectra of RNO 91, the FU Orionis star L1551 IRS5, RNO 90 (*top panel*), and (*b*) the FU Orionis star V1057 Cyg (*bottom panel*). Fluxes are given in arbitrary units. The estimated continuum levels are shown with solid lines. We attribute the weak, narrow absorption band in the spectrum of RNO 91 at 2139 cm^{-1} (4.68 μm) to the CO stretch of CO molecules frozen on the surfaces of grains in the disk around RNO 91 at 2139 cm^{-1} (4.68 μm) to the CO stretch of CO molecules frozen on the surfaces of grains in the disk around RNO 91. A broad, weak absorption band at 2165 cm^{-1} associated with XCN also may be present in this spectrum. The spectrum of L1551 IRS5 appears very similar to the RNO 91 spectrum. We detected no evidence of absorption at 2165 or 2139 cm^{-1} in the spectra of both RNO 90 and V1057 Cyg.

gests the feature is real. We performed a χ^2 test on these 12 spectral points to check the quality of the "fit" to the continuum. The calculation, which yields $\chi^2 = 21.2$, suggests that we might expect to obtain this set of measurements of the continuum only ~3% of the time. In other words, the χ^2 test indicates a ~97% likelihood that this consecutive string of 12 spectral points represents a real absorption band. We see no evidence of any absorption features at either 2165 or 2139

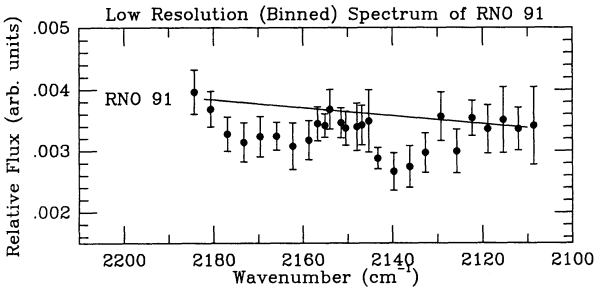

FIG. 3.—Calibrated 2187–2107 cm^{-1} spectra of RNO 91. Data are binned to half the spectral resolution of that plotted in Fig. 2.

cm^{-1} in the 2187–2107 cm^{-1} spectra of RNO 90 (Fig. 2*a*) or of the FU Orionis star V1057 Cyg (Fig. 2*a* and Tegler et al. 1993b). The absence of the absorption band at 2165 cm^{-1} in both of these spectra suggests that this feature is not systemic. An identical χ^2 test on the RNO 90 spectrum yields $\chi^2 = 9.22$, indicating this is a good fit to the continuum at the 80% confidence level. The small dips below the continuum near 2160 cm^{-1} and 2130 cm^{-1} may be the signature of gaseous CO in the RNO 90 spectrum; however, the limited signal-to-noise in this data does not permit us to evaluate this possibility.

We interpret the absorption bands at 3250 and 2139 cm^{-1} in the spectra of RNO 91 as due to frozen water and frozen carbon monoxide components, respectively, on the surfaces of dust grains along the line of sight to RNO 91 (see Tielens et al. 1991 for a detailed discussion of CO bands). The absorption band near 2165 cm^{-1} may arise from a —CN containing material known as XCN in the literature (Lacy et al. 1984; Tegler et al. 1993a). Further observations are necessary to verify the identity of this absorption band.

These absorption bands allow us to calculate column densities along the line of sight to RNO 91 as well as the relative abundance of absorbers, e.g., N_{CO}/N_{H_2O}. The column density of an absorbing species is given by

$$N = \frac{\Delta v_x \tau_x}{A_x}, \quad (1)$$

where x represents a molecular band, Δv_x represents the full width at half-maximum (FWHM) of the band z, τ_x represents the optical depth and A_x represents the integrated absorbance of the band. The optical depth at band center is obtained from our spectra. In particular,

$$\frac{I}{I_{ox}} = e^{-\tau_x}, \quad (2)$$

where I_o is the stellar intensity at band center and I is the intensity of light leaving the disk. Values for A_x and Δv_x are obtained from laboratory experiments. Column densities for the ice components along the lines of sight toward RNO 91 are given in Table 2. These column densities yield a relative abundance of frozen CO to frozen H_2O of $N_{CO}/N_{H_2O} = 0.13$ toward RNO 91. From our spectrum of RNO 90 we set an upper limit of 2.0×10^{17} cm^{-2} for the column density of frozen CO along the line of sight to RNO 90.

2.2. *Infrared Polarimetric Imaging*

We obtained images of RNO 91 through a broad-band K filter on 1990 April 10 and 11 with the 2.1 m telescope of the National Optical Astronomy Observatories on Kitt Peak. The infrared camera (IRIM; a 58 × 62 InSb array; 0.″71 pixel width) and polarizer (SLOPOL), as well as our observing and analysis techniques for collecting four-image polarimetric suites and obtaining Stokes parameters therefrom, are described in Weintraub et al. (1992). Our observing procedure was to make sets of polarized images of the target object, interspersed with identical sets on polarimetric reference sources and unpolarized standard stars and on sky. Each image set, or suite, consists of four separate images taken at 22.°5 intervals of the half-wave plate polarizer. The polarized nebula OH 231.8+4.2 was observed (1) in a large aperture and compared with the PA = 110° results of Heckert & Zeilik (1983) and Heckert & Smith (1988) and (2) at high resolution and compared with published maps of Dougados et al. (1990) to determine the absolute polarization position angles. We estimate an uncertainty of about 5° in our determination of the absolute position

TABLE 2

COLUMN DENSITIES OF ICES IN THE DISK OF RNO 91

Molecule	Band Width ($\Delta\nu$) (cm^{-1})	Reference	Absorbance (A) (cm molecule^{-1})	Reference	τ	Column Density (N) (molecules cm^{-2})
H_2O	335	[a]	2.0×10^{-16}	[a]	1.29	2.2×10^{18}
XCN	20	[a]	$2\text{–}4 \times 10^{-17}$	[a]	≤ 0.19	$\leq 1\text{–}2 \times 10^{17}$
CO (2139 cm^{-1})	11	[b]	1.0 and 1.7×10^{-17}	[c]	0.33	2.8×10^{17}

[a] d'Hendecourt & Allamandola 1986.
[b] From RNO 91 spectrum.
[c] We assume the CO band is composed of equal amounts of broad and narrow components. A values from Sandford et al. 1988.

angle. The infrared standards HD 129653 and BD +2°2957 served to calibrate the flux levels in the source images. We estimate the errors in photometry to be less than 10%. We used the absolute calibration given by Campins, Rieke, & Lebofsky (1985) to transform K magnitudes into flux densities. There is an uncertainty of approximately ±3% associated with the absolute calibration. The readout problem with this array that exists in data collected in 1988 and earlier had been fixed by the time these data were collected.

The net unpolarized image was constructed by co-adding the four polarimetric images obtained in a single suite of 15 s images (Fig. 4). In addition to these data, we utilized a 6″ diameter coronagraph to eliminate ghosting and saturation problems, in order to image RNO 91 for a total exposure of 980 s. The long exposure images (not shown) reveal no faint nebulosity beyond that seen in the unocculted images. In Figure 4, we see the same morphology as in the optical images. The southern peak (labeled S2 in Fig. 4, following the naming scheme in Schild et al. 1989) is clearly separated from the main peak of RNO 91 at K. This separation was not clear in the infrared images presented by Heyer et al. (1990) because of the readout problem. In addition to the southern extension, the K image also reveals extensions seen toward position angles 50° (extension H), 135°, 225° (extension S3), 260° (extension G1/G2), and 290° (extension P1/P2) in the optical nebulosity. In addition, the K image reveals nebulosity farther to the north and northeast of RNO 91 and farther to the southwest of the southern peak than previously detected. The imaged nebulosity at K extends ~20″ east–west and ~24″ north–south, to a limit of 0.20 mJy per square arcsec.

The polarimetric vector map (Fig. 5), which was made from the individual 15 s images, reveals a set of concentric semicircles of centrosymmetric vectors in the vicinity and to the north of RNO 91. In these regions the amplitude of polarization is 5%–25%. In general, the polarization amplitude increases with increasing distance from RNO 91. This is the expected behavior where photons from the outer nebula are preferentially singly scattered while more multiply scattered

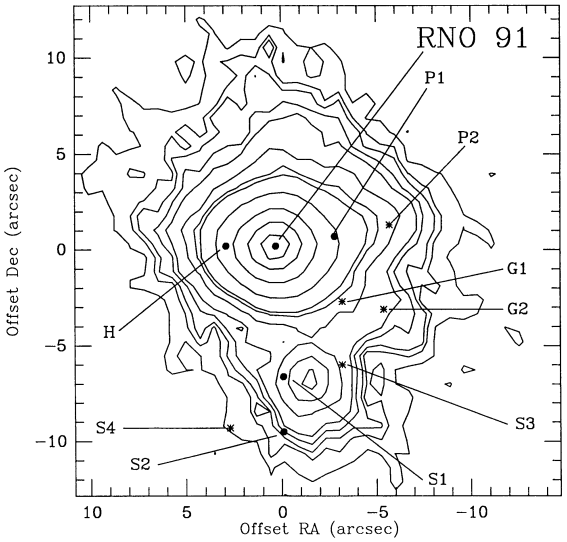

FIG. 4.—Flux density contour map made from K-band (2.2 μm) images of RNO 91 taken on 1990 April 10 at the NOAO 2.1 m telescope on Kitt Peak. Contour levels correspond to 0.20 (3 σ above the intensity level of the background sky), 0.29, 0.34, 0.43, 0.52, 0.77, 1.0, 1.2, 2.6, 8.6, 29, and 58 mJy per square arcsec. Peaks and extensions are labeled according to scheme adopted in Schild et al. (1989). One arcsecond is equivalent to 170 AU at the distance of RNO 91. The offset position (0, 0) in this map is placed at the position of the northern peak. The structures identified in Table 1 of Schild et al. (1989) in the nebulosity around RNO 91 are marked by filled circles (considered reflection nebulae by Schild et al.) and asterisks.

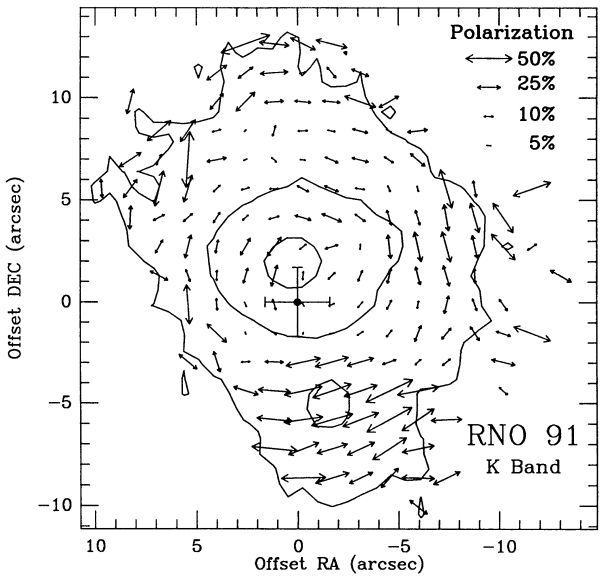

FIG. 5.—Individual pixel polarization vector map from K-band images of RNO 91 in which the lengths of the vectors are proportional to the percent polarization. The offset position (0, 0) in this map is placed at the position of the polarization centroid. Flux density contour levels correspond to 0.20, 1.0, and 29 mJy per square arcsec. The polarization centroid, marked as a solid dot with 1 σ bars, is located 0.″2 east and 1.″9 south of the RNO 91 intensity peak.

photons emerge from the inner nebula. In regions of the map where the percent polarization is low, multiple scattering probably is important; however, we cannot completely rule out the presence of other emission sources in these parts of the nebula. Between 6″ and 12″ south of RNO 91, the map reveals a set of more linearly aligned vectors representing polarization amplitudes in the range 30%–60%. Both parts of the vector map are nearly symmetric about an axis at position angle 190°. The simplest way to interpret a set of centrosymmetric vectors is to recognize that the perpendicular to each vector points back to the location of the emitted photons. The origin of the semicircles locates the position of the object that likely illuminates this reflection nebula and drives the molecular outflow. We have used the method described by Weintrub & Kastner (1993) to locate the centroid of the polarimetric map at $0\farcs2 \pm 1\farcs6$ west and $1\farcs9 \pm 1\farcs7$ south of the intensity peak of RNO 91. We estimate that the additional uncertainty in determining the absolute position angle for each vector adds an additional half arcsec error in both R.A. and decl. to the statistical errors presented. This result suggests that the intensity peak at $\lambda \leq 2.2$ μm may be a scattering peak and that the source of illumination is embedded in an optically thick region directly between the two main peaks (RNO 91 and S2) of the nebula. The errors on this measurement, however, are too large to permit us to draw a firm conclusion. The high polarization amplitudes associated with the southern intensity peak clearly mark it as a region of scattered light.

3. DISCUSSION

The observed polarimetric map of the RNO 91 nebula demonstrates that dust grains are abundant in the nebulosity around the central star. However, while the dust grains could be components of a circumstellar disk, they could also be entrained in the known molecular outflow. Thus, we next compare these observations to maps generated in Monte Carlo calculations of scattering by Whitney & Hartmann (1992, 1993). In our discussion, we assume the central illuminating source is located to the south of the northern infrared peak, i.e., that the northern and southern lobes are both scattering peaks.

Whitney & Hartmann have produced models of scattering in circumstellar disks (1992) and bipolar envelopes (1993) surrounding young stellar objects (YSOs). Their model results are plotted similarly to our observational data as sets of intensity contours overlaid with polarimetric vector patterns. The observed map of RNO 91 resembles very closely both the intensity contours and vector profiles in the bipolar model labeled $\mu = 0.3$ shown in Figure 3 of Whitney & Hartmann (1993) and also the disk model labeled $\mu = 0.5$ shown in Figure 8 of Whitney & Hartmann (1992). Both models (and our data) reveal a large, bright region of scattering (of moderate polarization amplitudes) to the north and a smaller, narrower, fainter region of high polarization to the south. In both models, the northern polar axis (seen in projection toward position angle 0°) is tilted $\sim 20°$–$30°$ out of the plane of the sky, toward the observer. In the bipolar model, the disk is not included. We see light scattered from dust only in the lobes. The northern lobe, which is seen in forward scattered light, is brighter than the southern lobe. In the disk model the lobes are not included and we see light scattered from dust in a large disk. In this case, the northern semidisk, which is seen in backward scattered light, is brighter than the southern semidisk. Thus, to match our observations, in which the northern part of the nebula is brighter, both models require that the northern axis of the RNO 91 system point toward the observer.

From radio observations of RNO 91, however, the northern outflow lobe is known to be redshifted and the southern outflow lobe blueshifted. Thus these radio observations require that the northern lobe be tilted away from the Earth; hence, neither model matches the near-infrared and radio observations.

A more realistic model would include scattering and absorption effects from both the outflow lobes and the disk. In the model depicted in Figure 6, the southern semidisk would be viewed in backscattered light through an obscuring outflow

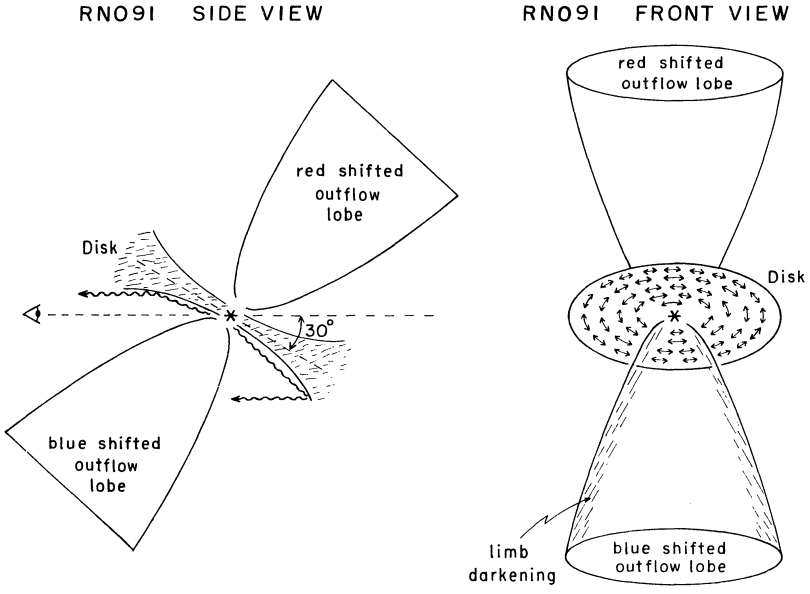

FIG. 6.—Illustrations of side and front views of RNO 91.

lobe. The northern semidisk, which is viewed in forward scattering, would suffer no additional extinction. With only a moderate amount of extinction, the scattered light from the southern semidisk could be substantially reduced to comparable or lesser brightness levels than the unextincted light scattered off the northern semidisk, thus yielding the morphology we observe. In the bipolar lobe case, however, the closer (blueshifted) lobe is already the brighter lobe, as seen in scattered light. This lobe suffers no additional extinction. Meanwhile, the fainter, more distant lobe suffers more extinction and becomes even fainter. Thus, the only way to reconcile these models with our data set is to conclude that we are observing a disk, and that to the south of the star the semidisk is seen through the obscuring outflow.

We interpret the K-band polarization map in exactly this way (Fig. 6). The northern portion of the scattering nebula is the part of the disk tilted toward Earth. Here, we view scattering off the bottom surface of a flared disk and we are able to see most of the disk, out to large distances from the YSO. Our view of the southern half of the disk is complicated by the presence of the blueshifted outflow that lies in front of this semidisk. The outflow has cleared away most of the dark cloud, creating a large bay in the cloud (Mathieu et al. 1988). As this outflow lies nearly in the plane of the sky, our view of the southern semidisk through the outflow lobe is more obscured when we look through the limbs of the outflow. Consequently, we observe only the central portion of the southern half of the disk.

If the northern intensity peak marks the location of the exciting star, we would conclude that this line of sight through the disk is optically thin at K as it permits a direct view to RNO 91. This result in turn would imply that $A_k < 1$ and, assuming the extinction law determined empirically by Becklin et al. (1978), $A_v < 10$. However, if as suggested by the polarization centroid location, the exciting star is located $\sim 2''$ directly south of the northern intensity peak, then this YSO would not be visible in the optical or near-infrared and we would conclude that $A_v > 10$.

The dislike structure around RNO 91, as projected on the plane of the sky, extends at least 10″ from the YSO. At a distance of 170 pc (Herbst & Warner 1981), this structure has a radius greater than 1700 AU. This is comparable in physical radius to the circularly symmetric near-infrared scattering nebula around T Tauri that Weintraub et al. (1992) suggest could be a flared disk viewed nearly pole-on.

In order to establish whether the ices seen along the line of sight toward RNO 91 are circumstellar or interstellar in origin, we need to investigate more closely related studies of these stars and of the dark cloud L43. Lynds (1962) assigned L43 to her highest opacity class. In fact, the line of sight to L43 shows very few other stars compared with adjacent portions of the sky (Elmegreen & Elmegreen 1979). The dark cloud has a high molecular density (1.5×10^5 cm^{-3}; Loren 1981) and contains a dense NH_3 core, offset slightly from the position of RNO 91 (Myers et al. 1988). Herbst & Warner (1981) concluded that the two optically visible T Tauri stars seen toward L43 (RNO 90 and RNO 91) lie just in front of, or only partially embedded within the cloud since each illuminates a reflection nebula. In I-band images, RNO 91 lies within a horseshoe-shaped region of lower extinction than the surrounding portion of L43 (Mathieu et al. 1988); nevertheless, the surface density of stars projected onto the bay is still only 10% that of the star field that surrounds L43. Mathieu et al. show that this bay coincides with the blue lobe of the ^{12}CO outflow and conclude that the outflow has disrupted the surrounding medium, displacing most—though possibly not all—of the intracloud material along our line of sight to RNO 91.

The intracloud environments of the Taurus, ρ Ophiuchi, and Corona Australis molecular clouds apparently contain large numbers of icy grains (Whittet et al. 1983; Tanaka et al. 1990; Chen & Graham 1993). As a result, absorption bands associated with frozen CO and H_2O are often seen toward embedded or background stars if the optical depths through the clouds toward these stars are above critical thesholds. For example, the critical depth ($A_{v,c}$) for the detection of frozen CO toward background stars seen through the Taurus clouds is $A_{v,c}(\mathrm{CO}) \simeq 8$ (Whittet et al. 1985); the critical optical depth for the detection of frozen water is $A_{v,c}(\mathrm{H_2O}) \simeq 3$ for Taurus (Whittet et al. 1988), $A_{v,c}(\mathrm{H_2O}) \simeq 15$ for Ophiuchus (Tanaka et al.), and $A_{v,c}(\mathrm{H_2O}) \simeq 6$ for Corona Australis (Chen & Graham). It is likely that $A_{v,c}(\mathrm{CO}) > A_{v,c}(\mathrm{H_2O})$ in all cases. Furthermore, as the critical thresholds in Taurus are so low, they may represent near minima values for dark clouds. If the L43 cloud is similar to Taurus, Corona Australis, and nearby ρ Ophiuchi, and if the intracloud optical depth toward RNO 91 is large enough, frozen CO and H_2O along the line of sight through L43 may be responsible for some or all of the absorption seen in these spectra of RNO 91.

The apparent similar locations of RNO 90 and RNO 91 in front of or near the front of L43 (Herbst & Warner 1981) permit us to employ our spectroscopic observations of RNO 90 as a test to determine whether a significant amount of intracloud material lies along the line of sight through L43 to this pair of T Tauri stars. The spectrum of RNO 90 reveals no evidence for frozen CO located in the L43 cloud along the line of sight to RNO 90. The absence of solid CO absorption in the RNO 90 spectrum suggests that the intracloud medium in L43 does not contain large numbers of ice-coated grains and/or that the intracloud A_v is small toward RNO 90. Since RNO 90 and RNO 91 are apparently located at relatively similar optical depths into L43, *most of the ices detected in the spectra of RNO 91 are probably located on grains in the circumstellar disk of RNO 91.*

We have compared our spectra of RNO 91 with spectra of other pre–main-sequence stars and laboratory analogs. The absorption band at 3250 cm^{-1} in the spectrum of RNO 91 shows an asymmetrical profile, i.e., a redward wing. Spectra of other pre–main-sequence stars also show bands at 3250 cm^{-1} with similar asymmetrical profiles (e.g., see Smith, Sellgren, & Tokunaga 1989). Laboratory spectra suggest a likely explanation for the shape of the asymmetrical band is that frozen H_2O molecules produce symmetrical absorption near 3250 cm^{-1} and hydrocarbons produce additional absorption redward of 3250 cm^{-1}, creating the redward wing (Duley & Williams 1981; Smith et al. 1989).

In laboratory experiments, Hagen, Allamandola, & Greenberg (1980) show that frozen CO has an absorption band at 2139 cm^{-1}. Laboratory experiments by Sandford et al. (1988) show that the CO band center, width, and integrated absorbance are sensitive to the composition of the matrix material surrounding the CO molecules. In particular, a narrow band (FWHM ~ 5 cm^{-1}) with center near 2139 cm^{-1} results from absorption by CO molecules surrounded by a matrix dominated by nonpolar molecules, such as CO or CO_2 molecules. For CO molecules in nonpolar environments Sandford et al. find the integrated absorbance $A_{\mathrm{nonpolarCO}} = 1.0 \times 10^{-17}$ cm

molecule^{-1}. A broad band (FWHM ~ 10 cm^{-1}) with center near 2135 cm^{-1} results from absorption by CO molecules surrounded by a polar matrix, such as H_2O molecules. For CO molecules in polar environments Sandford et al. find $A_{\text{polar CO}} = 1.7 \times 10^{-17}$ cm molecule^{-1}. Tielens et al. (1991) present astronomical spectra indicating CO absorption in a polar matrix (e.g., AFGL 2136) and other spectra indicating CO absorption in a nonpolar matrix (e.g., NGC 7538 IRS 9). Spectra of astronomical sources also show frozen CO bands that are composed of similar amounts of broad and narrow components (e.g., spectra of Elias 18 show a frozen CO band with FWHM of 11 cm^{-1} and band center at 2140 cm^{-1}, see Sandford et al.). The band center and FWHM also are dependent on the matrix temperature. In particular, Sandford et al. present laboratory experiments that show the CO band center shifts from 2137 to 2134 cm^{-1} as the temperature of a H_2O:CO = 20:1 frozen mixture changes from 10 to 150 K. The CO absorption band in the spectrum of RNO 91, which has an 11 cm^{-1} FWHM and a center at 2139 cm^{-1}, is very similar to the frozen CO absorption band seen in the spectrum of Elias 18. We assume that the broad and narrow components contribute equally to the CO absorption band in the spectrum of RNO 91.

Laboratory experiments involving the components under conditions similar to the environment around pre–main-sequence stars show that frozen H_2O sublimates at temperatures near 150 K (Sandford & Allamandola 1988). These experiments also show that frozen CO in nonpolar matrices sublimates at temperatures near 30 K while frozen CO in polar matrices sublimates at temperatures as high as 150 K. Within a circumstellar disk around a T Tauri star, temperatures below 150 K would likely be found at distances beyond ~ 10 AU from the photosphere. Thus our observations of frozen CO and H_2O suggest we are probing regions in the disk around RNO 91 colder than 150 K at distances of perhaps 10–1700 AU from the central star. This material may therefore represent icy, precometary grains orbiting this T Tauri star.

Tielens & Allamandola (1987) examined the abundance of frozen CO to frozen H_2O in the material along the line of sight toward seven embedded protostars and found $0.02 \leq N_{CO}/N_{H_2O} \leq 0.22$. These results are consistent with those of Tielens et al. (1991), who found $0.01 \leq N_{CO}/N_{H_2O} \leq 0.18$ for an overlapping sample of 18 protostars. Balsiger et al. (1986) determined $CO/H_2O = 0.05$ for comet Halley using data collected by the European spacecraft *Giotto*. The similarity in the abundance of frozen CO to frozen H_2O in circumstellar shells around protostars, the disk around RNO 91, and comet Halley suggests some icy grains may not be subject to extensive thermal processing before incorporation into comets; however, more observations of protostars, comets, and especially T Tauri stars will be necessary before we can draw more firm conclusions about the extent of processing of icy grains in preplanetary disks.

4. CONCLUSIONS

We have mapped the infrared polarization field in the nebula surrounding the T Tauri star RNO 91 and have determined that this scattering nebula is most likely a disklike structure with a radius of ~ 1700 AU. Our spectroscopic observations of RNO 90 reveal no evidence for frozen CO in front of or very near the front of L43. This leads us to conclude that L43 contributes very little intracloud extinction along the lines of sight toward either star. Thus, the frozen H_2O, CO, and possibly XCN mantled dust grains that produce the absorption bands we observe in the spectrum of RNO 91 most likely reside in a circumstellar disk.

We thank Barbara Whitney for valuable discussions concerning her scattering models. We also thank Tim Brooke and Alan Tokunaga for collecting the 3 μm spectra. This research is supported by NASA Origins of Solar Systems Program grants to Vanderbilt University and the University of Notre Dame as well as the Jesse Jones Foundation at the University of Notre Dame and the University Research Council of Vanderbilt University.

REFERENCES

Balsiger, H., et al. 1986, Nature, 321, 330
Becklin, E. E., Mathews, K., Neugebauer, G., & Willner, S. P. 1978, ApJ, 220, 831
Campins, H., Rieke, G. H., & Lebofsky, M. J. 1985, AJ, 90, 896
Chen, W. P., & Graham, J. A. 1993, ApJ, 409, 319
Cohen, M. 1975, MNRAS, 173, 229
d'Hendecourt, L. B., & Allamandola, L. J. 1986, A&AS, 64, 453
Dougados, C., et al. 1990, in Astronomy with IR Arrays, ed. R. Elston (ASP Conf. Ser. 14), 152
Duley, W. W., & Williams, D. A. 1991, MNRAS, 196, 269
Elmegreen, D. M., & Elmegreen, B. G. 1979, AJ, 84, 615
Hagen, W., Allamandola, L. J., & Greenberg, J. M. 1980, A&A, 86, 1
Heckert, P. A., & Smith, P. S. 1988, AJ, 95, 873
Heckert, P. A., & Zeilik, M. 1983, MNRAS, 202, 531
Herbst, W., & Warner, J. W. 1981, AJ, 86, 885
Heyer, M. H., Ladd, E. F., Myers, P. C., & Campbell, B. 1990, AJ, 99, 1585
Lacy, J. H., Baas, F., Allamandola, L. J., Persson, S. E., McGregor, P. J., Lonsdale, C. J., Geballe, T. R., & Vand de Bult, C. E. P. 1984, ApJ, 276, 533
Levreault, R. M. 1988, ApJ, 330, 897
Loren, R. B. 1981, AJ, 86, 69
Lynds, B. T. 1962, ApJS, 7, 1
Mathieu, R. D., Benson, P. J., Fuller, G. A., Myers, P. C., & Schild, R. E. 1988, ApJ, 330, 385
Mumma, M., Weissman, P., & Stern, S. A. 1993, in Protostars and Planets III, ed. E. Levy & J. Lunine (Tucson: Univ. Arizona Press), 1177
Myers, P. C., Heyer, M., Snell, R. L., & Goldsmith, P. F. 1988, ApJ, 324, 907
Sandford, S. A., & Allamandola, L. J. 1988, Icarus, 76, 201
———. 1990, Icarus, 87, 188
Sandford, S. A., Allamandola, L. J., Tielens, A. G. G. M., & Valero, G. J. 1988, ApJ, 329, 498
Schild, R., Weir, N., & Mathieu, R. D. 1989, AJ, 97, 1110
Smith, R. G., Sellgren, K., & Tokunaga, A. T. 1989, ApJ, 344, 413
Tanaka, M., Sato, S., Nagata, T., & Yamamoto, T. 1990, ApJ, 352, 724
Tegler, S. C., Weintraub, D. A., Allamandola, L. J., Sandford, S. A., Rettig, T. W., & Campins, H. 1993a, ApJ, 411, 260
Tegler, S. C., Weintraub, D. A., & Rettig, T. W. 1993b, in preparation
Tielens, A. G. G. M. 1989, in Interstellar Dust, ed. A. G. G. M. Tielens & Allamandola (Dordrecht: Kluwer), 239
Tielens, A. G. G. M., & Allamandola, L. J. 1987, in Physical Processes in Interstellar Clouds, ed. G. E. Morfill & M. Scholer (Dordrecht: Reidel), 333
Tielens, A. G. G. M., Tokunaga, A. T., Geballe, T. R., & Baas, F. 1991, ApJ, 381, 181
Tokunaga, A. T., Smith, R. G., & Irwin, E. 1987, in Infrared Astronomy with Arrays, ed. C. G. Wynn-Williams & E. E. Becklin (Honolulu: Univ. Hawaii), 367
Weintraub, D. A., & Kastner, J. H. 1993, ApJ, 411, 767
Weintraub, D. A., Kastner, J. H., Zuckerman, B., & Gatley, I. 1992, ApJ, 391, 784
Whitney, B. A., & Hartmann, L. 1992, ApJ, 395, 529
———. 1993, ApJ, 402, 605
Whittet, D. C. B., Bode, M. F., Longmore, A. J., Adamson, A. J., McFadzean, A. D., Aitken, D. K., & Roche, P. F. 1988, MNRAS, 233, 321
Whittet, D. C. B., Bode, M. F., Longmore, A. J., Baines, D. W. T., & Evans, A. E. 1983, Nature, 303, 218
Whittet, D. C. B., Longmore, A. J., & McFadzean, A. D. 1985, MNRAS, 216, 45P
Willner, S. P., et al. 1982, ApJ, 253, 174